SUPPORTING INFORMATION

Concentration-Tailored Interphase Engineering in Solid-State Polymer Electrolytes for High-Voltage Lithium Metal Batteries

Honghui Peng[1], Dong Liu[1], Zian Wang[1], Libao Chen[1], Chunxiao Zhang[1], Kunyun Yan[1,], Jialin Lin[1,*] and Weifeng Wei[1]*

[1] State Key Laboratory of Powder Metallurgy, Central South University, Changsha, Hunan, P. R. China, 410083

E-mail: 213307003@csu.edu.cn (J. Lin)

kunyun0206@163.com (K. Yan)

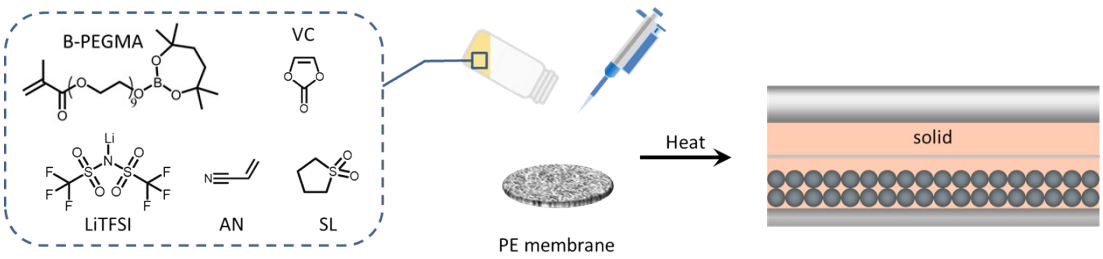

Figure S1. In-situ Polymerization Solid-State Battery Fabrication Mechanism Diagram.

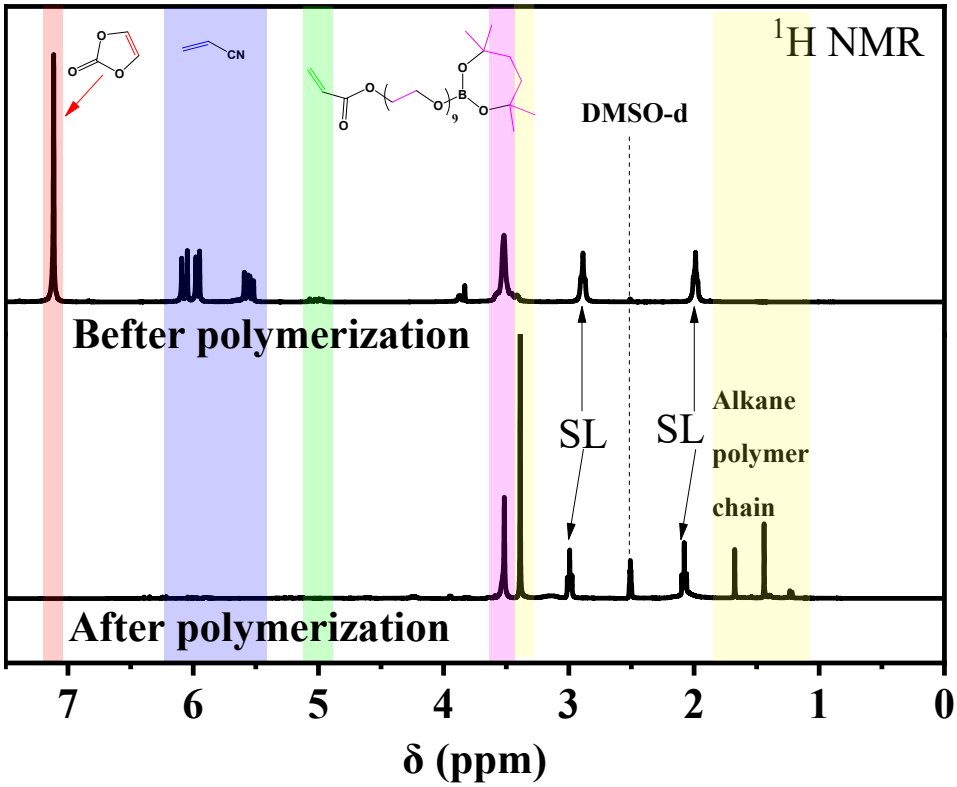

Figure S2. The^{1}H-NMR spectra of the electrolyte before and after polymerization.

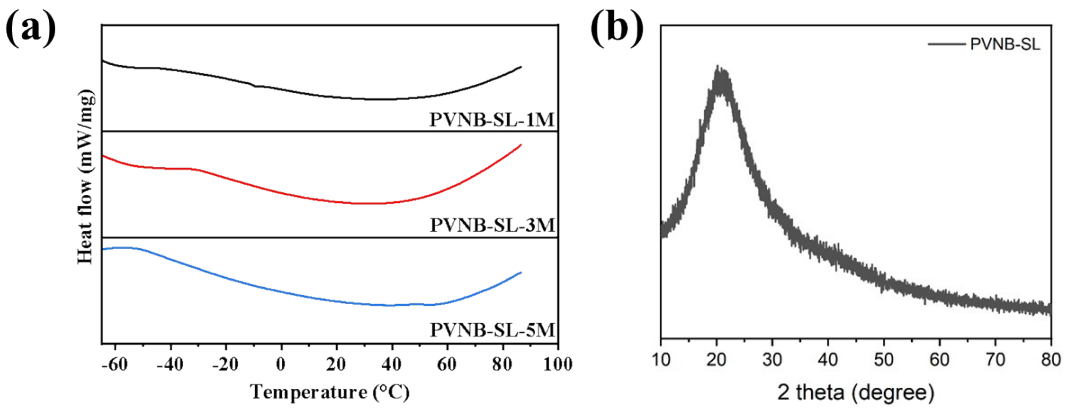

Figure S3. (a) The DSC curves of PVNB-SL electrolytes with varying lithium salt concentrations. (b) XRD spectrum of PVNB-SL electrolyte membrane.

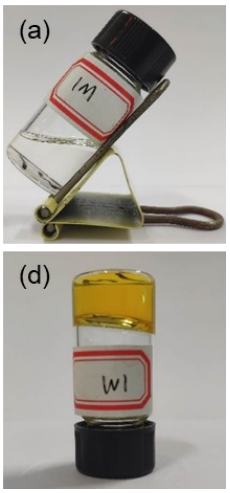

Figure S4. Optical images of PVNB-SL electrolytes before polymerization and after polymerization.

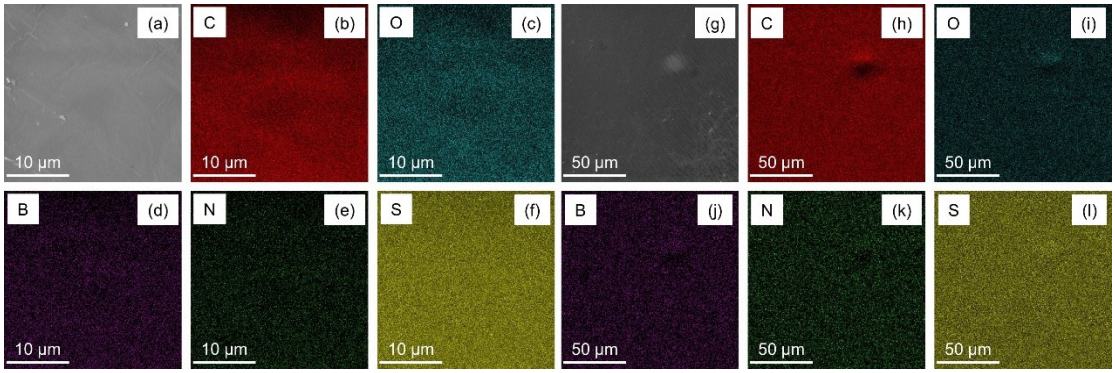

Figure S5. The SEM images of the (a) surface and (g) interior of the PVNB-SL electrolyte membrane; (b-f) Surface and (h-l) interior EDS mapping of PVNB-SL electrolyte membrane.

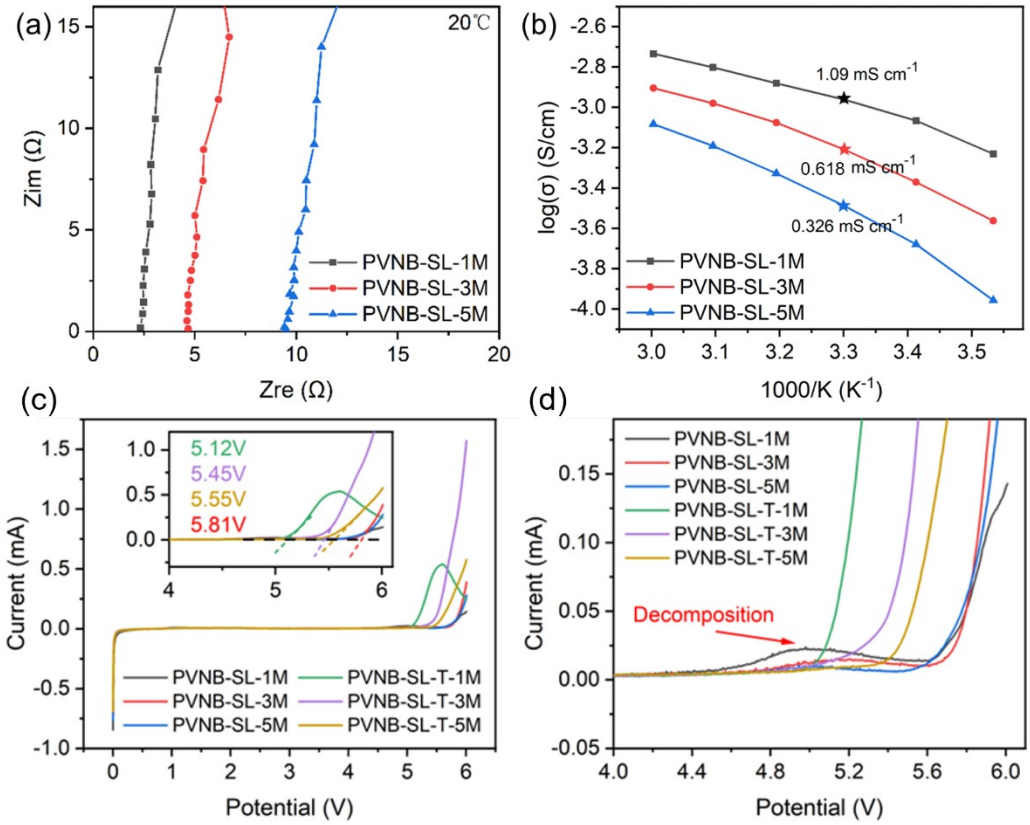

Figure S6. (a-b) The ionic conductivity of different electrolyte systems. (c) Electrochemical stability window and (d) partial view of electrolytes with different lithium salt concentrations.

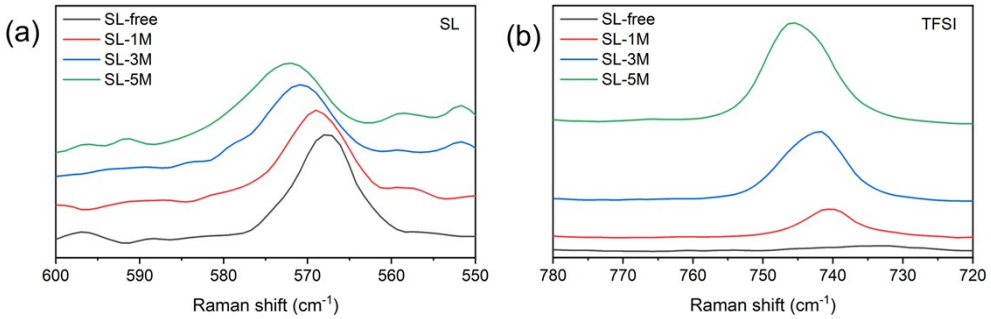

Figure S7. Raman spectra of SL solutions with different lithium salt concentrations.

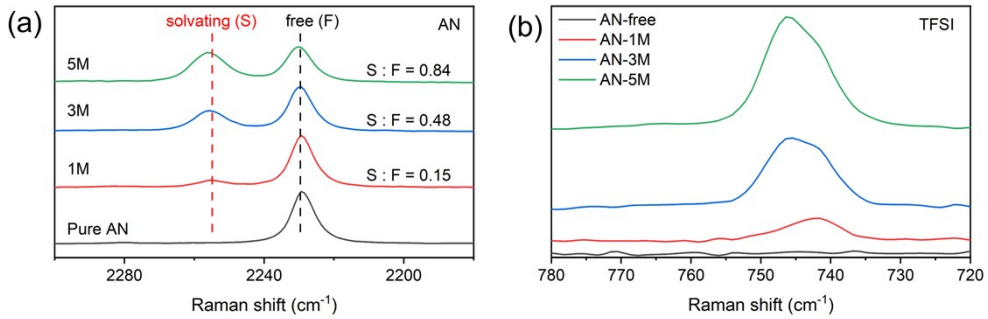

Figure S8. Raman spectra of AN solutions with varies lithium salt concentrations (a) and (b).

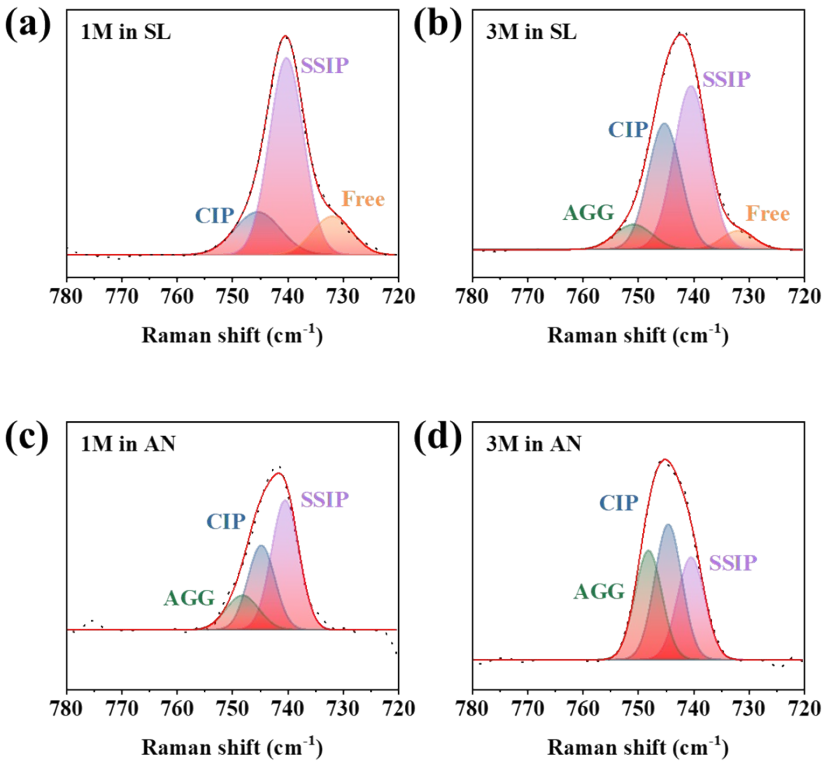

Figure S9. Raman spectra of SL/AN solutions with different lithium salt concentrations.

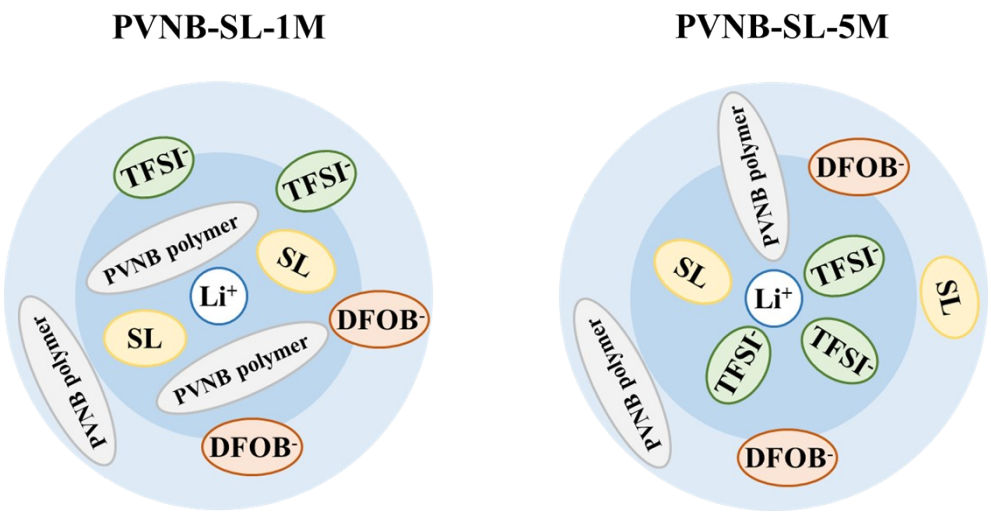

Figure S10. The schematic diagram of Li^+ solvation structure.

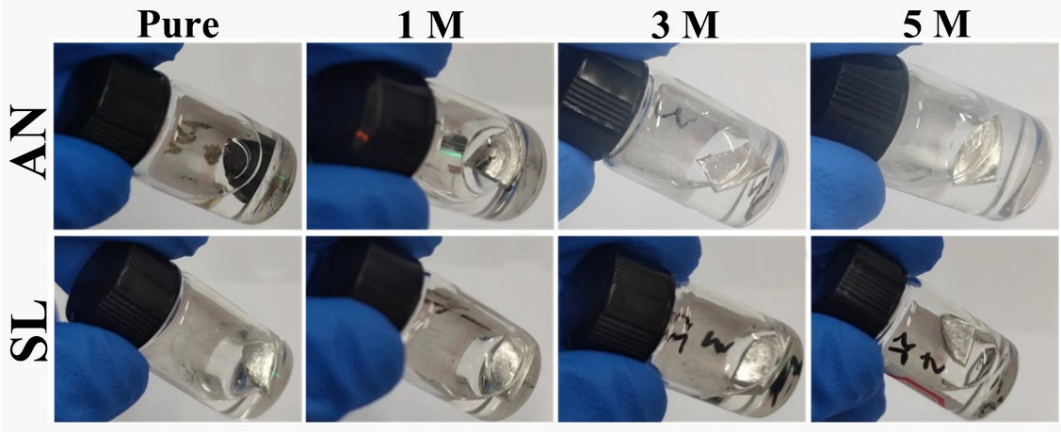

Figure S11. Optical photos of Li metal aging in AN and SL with different lithium salt concentrations before aging at 60 ℃.

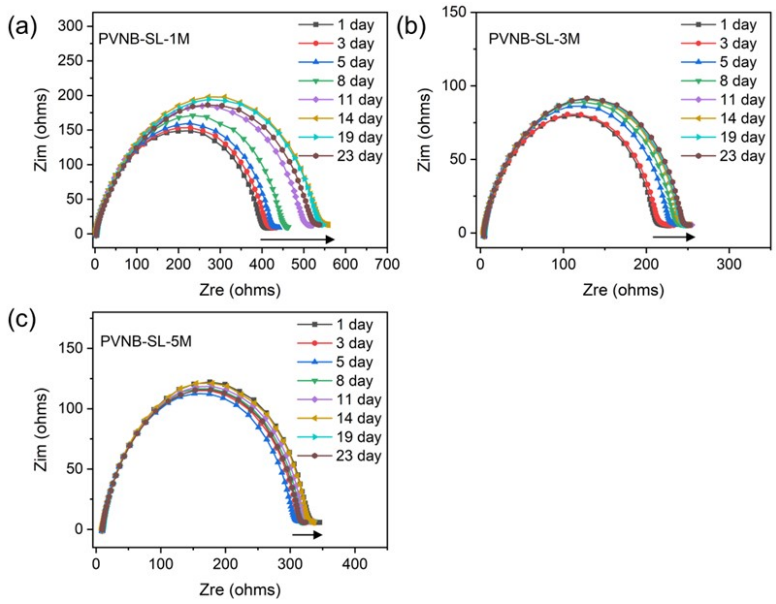

Figure S12. Evolution of impedance of Li||Li cells using (a) PVNB-SL-1M, (b) PVNB-SL-3M and (c) PVNB-SL-5M.

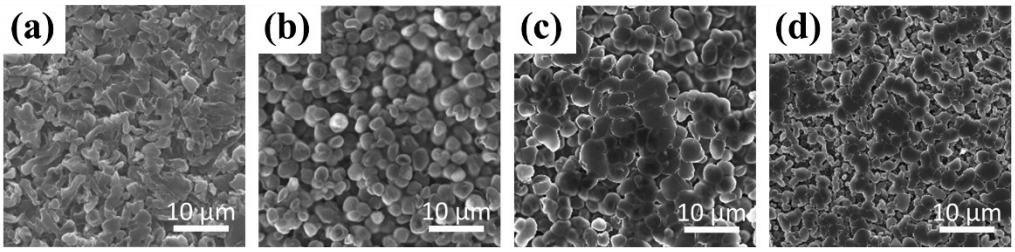

Figure S13. The deposition morphology and cross-sectional view of Li metal on the copper foil surface in (a) LE, (b) PVNB-SL-1M, (c) PVNB-SL-3M and (d) PVNB-SL-5M at 0.33 mA cm^{-2}, 2 mAh cm^{-2}.

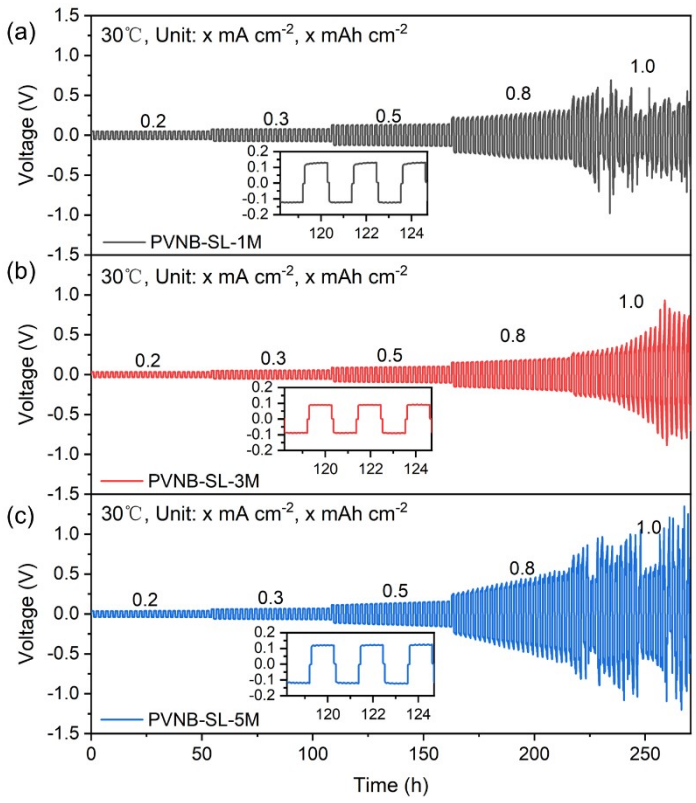

Figure S14. Cycling tests of Li-symmetric cells at different current densities using (a) PVNB-SL-1M, (b) PVNB-SL-3M and (c) PVNB-SL-5M.

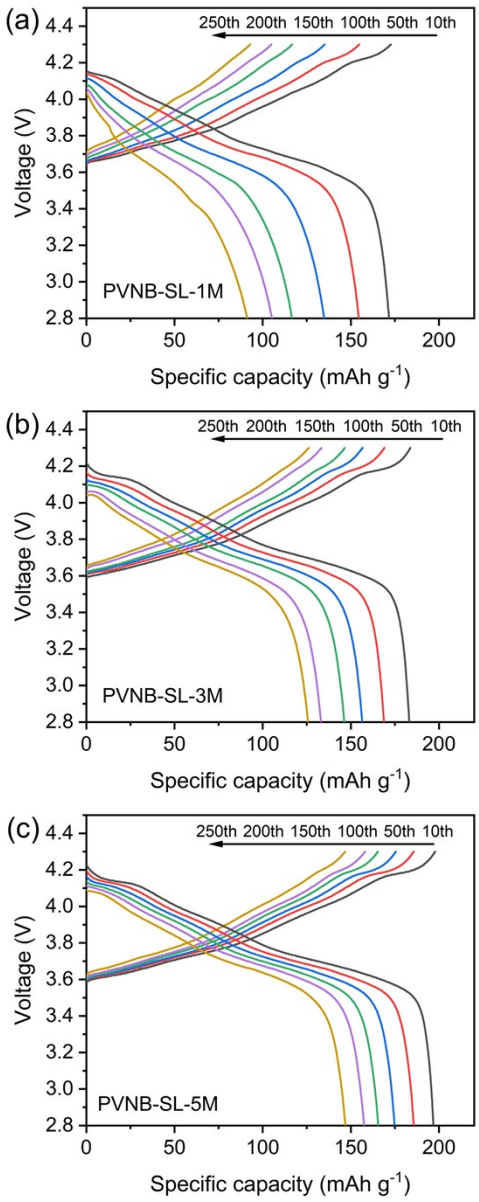

Figure S15. Specific capacity-voltage curves of (a) PVNB-SL-1M, (b) PVNB-SL-3M, (c) PVNB-SL-5M.

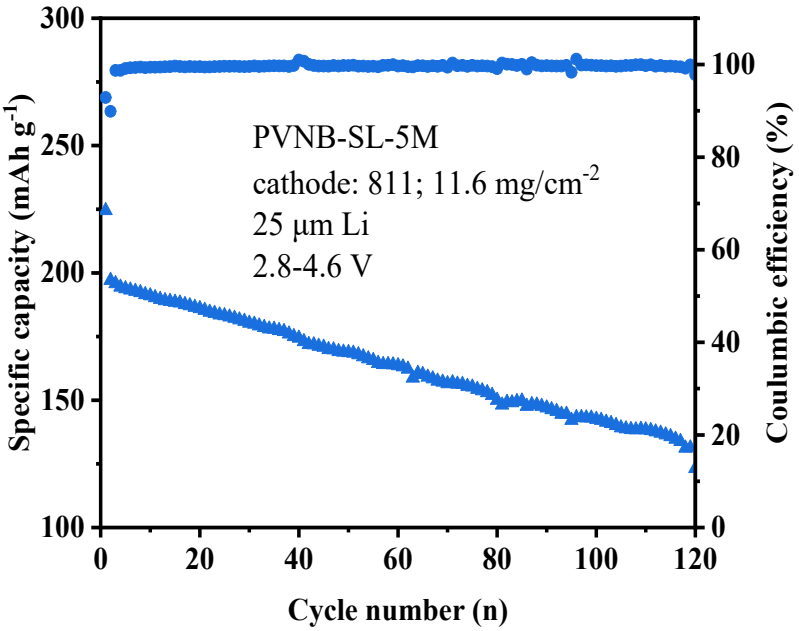

Figure S16. The cycling performance of NCM811||PVNB-SL-5M||Li cell using high-loading cathode and thin Li metal anode.

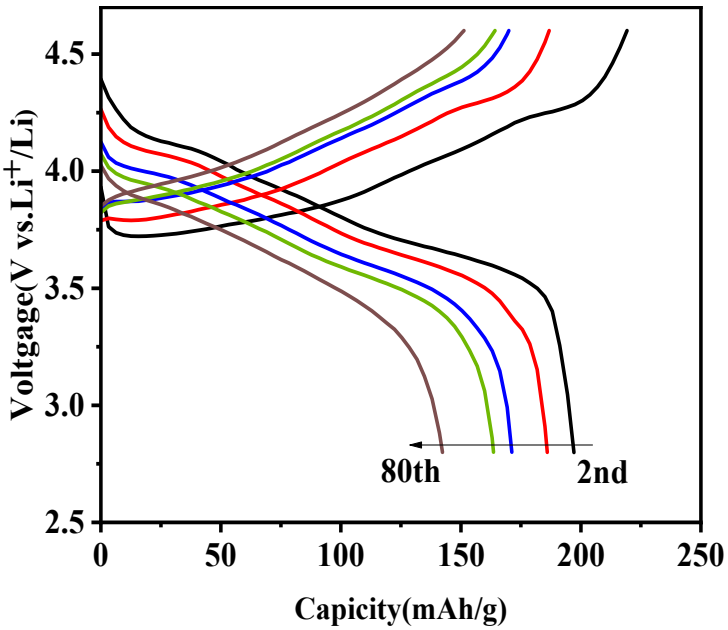

Figure S17. The charging-discharging curves of NCM811||PVNB-SL-5M||Li cell using high-loading cathode and thin Li metal anode.

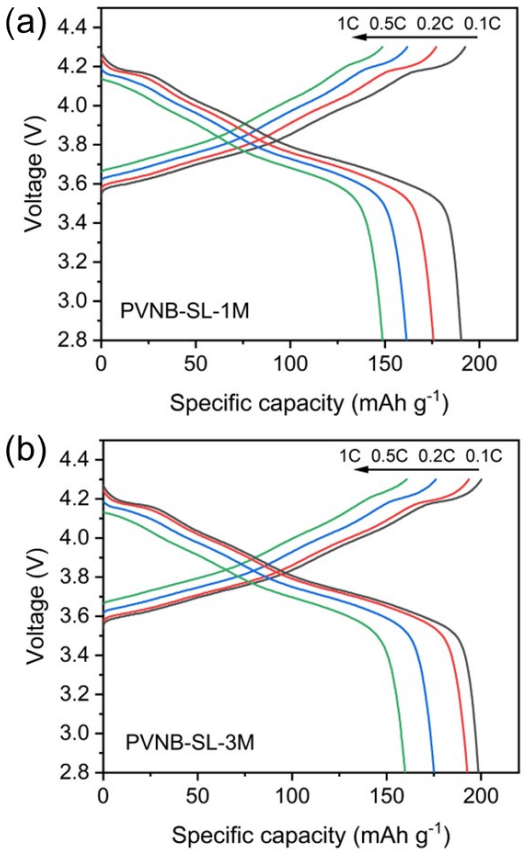

Figure S18. The charge-discharge curves of solid-state cells at 30 ℃ of (a) PVNB-SL-1M, (b) PVNB-SL-3M.

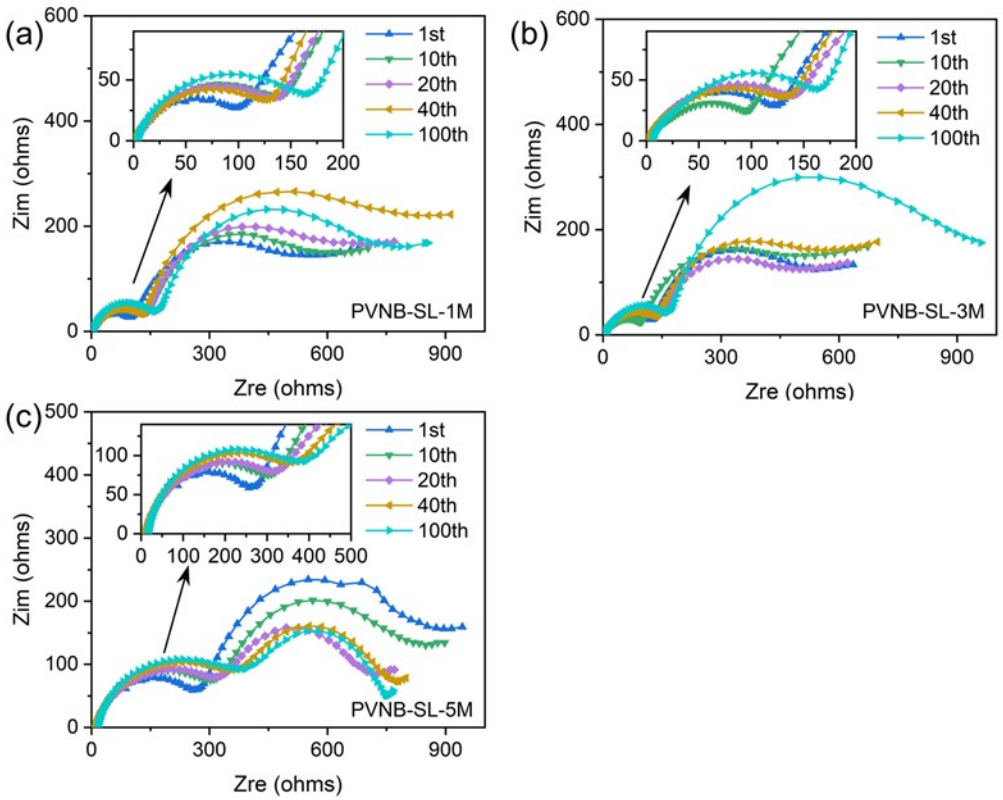

Figure S19. Electrochemical impedance of solid-state cells at different cycles using (a) PVNB-SL-1M, (b) PVNB-SL-3M, (c) PVNB-SL-5M.

Table S1. Table of electrolyte composition (units = g)

Electrolyte	VC	AN	B-PEGMA	SL	LiTFSI	LiDFOB
PVNB-SL-1M	1.4	0.6	0.5	0.5	0.678	0.0377
PVNB-SL-3M					2.034	0.113
PVNB-SL-5M					3.391	0.189
PVNB-SL-T-1M					0.678	--
PVNB-SL-T-3M					2.034	--
PVNB-SL-T-5M					3.391	--

Table S2. Li-ion transference number of PVNB-SL electrolyte with different concentrations.

Electrolyte	R_0	R_{ss}	I_0	I_{ss}	t_{Li^+}
PVNB-SL-1M	296.6	303.7	30.42	28.8	0.71
PVNB-SL-3M	138.1	142.7	62.83	59.44	0.82
PVNB-SL-5M	328.5	354.9	27.86	25.55	0.84

Table S3. Comparison of cycle performance of solid-state cells.

Electrolyte	Initial capacity (mAh g^{-1})	Specific capacity (mAh g^{-1})/Capacity retention (100 cycles)	Specific capacity (mAh g^{-1})/Capacity retention (250 cycles)
PVNB	151.0	111.1(73.6%)	-
PVNB-SL-1M	171.8	134.9 (78.5%)	95.0 (55.0%)
PVNB-SL-3M	186.9	156.5 (83.7%)	125.7 (67.2%)
PVNB-SL-5M	195.0	170.9 (87.7%)	142.2 (73.0%)

Table S4. The fitting results of the impedance spectrum (units = Ω cm^{-2}).

Cycle number	PVNB-SL-1M			PVNB-SL-3M			PVNB-SL-5M		
	R_b	R_a	R_c	R_b	R_a	R_c	R_b	R_a	R_c
1st	2.1	95.3	527.5	4.6	114.4	477.1	10.5	244.2	722.6
10th	2.2	131.6	536.7	4.2	92.58	479.7	11.3	271.6	641.2
20th	2.75	129.6	582.8	4.1	128.4	556.9	11.1	265.6	514.4
40th	2.16	121	777.5	4.5	150.2	758.1	11.41	283.8	541.5
100th	3.05	157.1	649.8	4.6	172.2	733.2	13.6	309	479.2